JOURNAL OF THE AMERICAN CHEMICAL SOCIETY

(Registered in U. S. Patent Office)

VOLUME 83 JANUARY 16, 1961 NUMBER 1

PHYSICAL AND INORGANIC CHEMISTRY

[CONTRIBUTION FROM THE DEPARTMENT OF CHEMISTRY, UNIVERSITY OF CALIFORNIA, BERKELEY 4, CALIFORNIA]

Large Tunnelling Corrections in Chemical Reaction Rates.[1] II

BY HAROLD S. JOHNSTON AND DONALD RAPP

RECEIVED APRIL 26, 1960

In terms of certain lengths near the saddlepoint of an activated complex relative to the de Broglie wave length of the atom being transferred, the reaction coördinate of bimolecular atom-transfer reactions is profitably classified as: (1) essentially classical, (2) essentially separable or (3) non-separable. In terms of the location of the saddlepoint and energy–distance curvatures through the saddlepoint, simple general rate expressions for case 1 and case 2 are given, including a small degree of tunnelling, utilizing the recent general method (ref. 6) of evaluating the configuration integral of any molecule. Hydrogen atom transfer reactions below several hundred degrees centigrade are in the region of non-separable reaction coördinates. For these cases more information about the potential energy surface is needed than the saddlepoint geometry and curvatures. Sample calculations using the Sato-potential energy surface for H_3, as evaluated by Weston, illustrate an approximate method for treating non-separable reactions, including large degrees of non-separable tunnelling. The hydrogen–deuterium isotope effect in reactions of methyl radicals with hydrocarbons is worked out in detail, and this method of handling large degrees of tunnelling appears to agree with the experimental data over a wide temperature range (although there is large experimental error).

Introduction

In a previous article[2] referred to as T-I we pointed out the anomalies in the rates of hydrogen-atom abstraction reactions by methyl radicals. The data clearly required some tunnelling correction, and yet such a correction based on a one-dimensional Eckart potential along the classical reaction path greatly overestimated the rate. The comparison of H_3C-H-D and H_3C-D-H also indicated these reactions have about equal tunnelling factors with tunnelling occurring along modes of motion different from the normal modes of small vibration theory. We developed the thesis that the usual procedure of treating the reaction coördinate as a one-dimensional, separable coördinate cannot be employed if the de Broglie wave length Λ^* for the atom being transferred is large compared to the linear portions (both in the R_1–R_2 plane and along the potential energy profile) of the potential energy surface around the saddlepoint.

The meaning of these restrictions is well brought out by considering the classical reaction path in the R_1–R_2 plane, AOB in Fig. 1, and by considering the energy profile along this path, AOB in Fig. 2. Fig. 1 shows several features of a conventional potential energy surface[3] with contour lines of constant potential energy, the "classical reaction path" AOB, and with several straight lines drawn in. The potential energy[4] along the "classical reaction path" is given by AOB in Fig. 2, and an extended parabola based on the curvature at 0 is given by POQ.

It is convenient to recognize three special cases, although in fact the three situations flow continuously from one to another. (1) *The reaction coördinate is essentially classical:* The criterion is that the de Broglie wave length Λ^* of the atom being transferred is short compared to the essentially linear portion of AOB near O in Fig. 1 and is short compared to the essentially flat-topped portion of AOB near O in Fig. 2. (2) *The reaction coördinate is separable but not classical:* In an area near the saddlepoint O in Fig. 1 the changes in potential energy on the surface may be adequately approximated by

$$2\Delta V = F_{11}(\Delta R_1)^2 + F_{22}(\Delta R_2)^2 + 2F_{12}\Delta R_1 \Delta R_2 \quad (1)$$

where Δ's refer to displacements from the saddlepoint. The criterion for the separability of the reaction coördinate is that each dimension of this

(1) In part from Ph.D. thesis by D. Rapp, Univ. of Calif., 1959.

(2) H. S. Johnston, *Advances in Chemical Physics*, 3, in press (1960).

(3) S. Glasstone, K. J. Laidler and H. Eyring, "Theory of Rate Processes," McGraw–Hill Book Co., New York, N. Y., 1941.

(4) The features of Fig. 2 are to scale and are based on Dr. Ralph Weston's Sato potential for the H_3 activated complex, R. E. Weston, *J. Chem. Phys.*, **31**, 892 (1959).

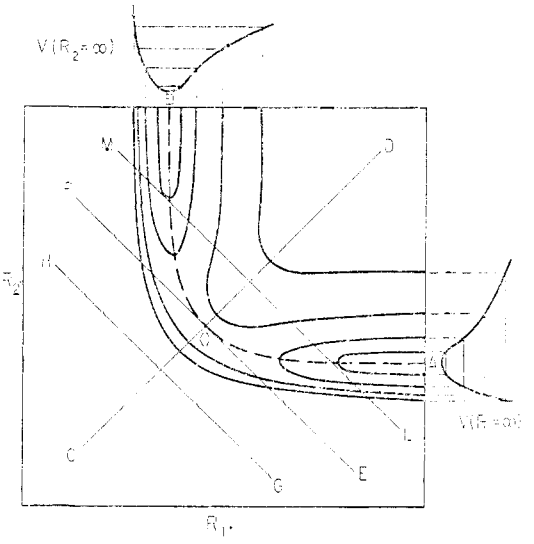

Fig. 1.—Portion of a potential energy contour map for atom transfer reaction, where the activated complex is symmetrical with respect to bond lengths R_1 and R_2 and to force constants along these bonds. AOB is the "reaction path"; COD is the extended symmetric stretch normal mode; EOF is the *extended* reaction coordinate or reaction normal mode; GH is a line parallel to EOF at a "shorter crossing distance"; and LM is a line parallel to EOF at a "longer crossing distance."

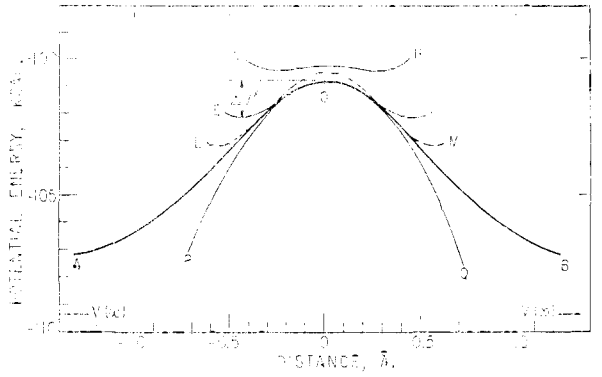

Fig. 2.—Potential energy profiles along various lines in Fig. 1. Energy and distance are to scale for the H activated complex according to Weston's calculations of a Sato potential. The line POQ is the extended parabola that has the same curvature $-F^*$ as EOF at O. In fitting an Eckart function to curve EOF, the parameters are the negative curvature F^* and the energy difference ΔV^*.

area be long compared to Λ^*; that is, the dimensions of the quadratic region near the saddlepoint O must be large compared to Λ^*. The region over which the parabola POQ in Fig. 2 corresponds adequately to the reaction path AOB may be used to estimate the extent of the quadratic region; it is about ± 0.3 Å. for H_3. (3) *The reaction coördinate is non-separable:* The criterion is simply that the de Broglie wave length Λ^* is larger than the dimensions of the quadratic region. The de Broglie wave length, $h(2\pi mhT)^{-1/2}$, for a hydrogen atom at 300°K. is 1.01 Å. and at 500°K. is 0.78 Å. Thus reactions involving hydrogen transfer at temperatures within several hundred degrees of room temperature fall into the third category!

This article develops an approximate method for treating special cases of reactions which fall under group 3. Further and more fundamental work on this topic is underway.[5]

Classical Reaction Coördinate.—For a flat topped barrier (that is, flat relative to Λ^*) it is convenient to consider two sub-classifications: (a) all internal vibrations are also classical and (b) the other internal vibrations are quantized. For the reaction Ax + B = A + xB, the completely classical problem can be set up with no conceptual difficulties. If reactants Ax and B have an equilibrium distribution over their excited molecular states, then properties of the activated complex with respect to arrival of reactants should be averaged over equilibrium distributions. If an imaginary line is placed through and normal to the saddlepoint (point O in Fig. 2), the flux of systems through this line from the side of reactants is

$$R = \frac{Q^{\pm}}{Q_{Ax}Q_B}[Ax][B]\frac{1}{Q_*}\frac{kT}{h}e^{-E_0/RT} \qquad (2)$$

where Q_{Ax} and Q_B are partition functions for reactants, $Q^{\pm}$ is the complete partition function ($3N$ dimensional) for the activated complex, Q_* is the phase integral for the reaction coördinate, $(1/h)\int_{-\delta/2}^{\delta/2}\int_{\infty}^{\infty} e^{-H^*/kT}\,dqdp$, and the other terms are conventional. Eyring,[3] reasonably enough, prefers to express both $Q^{\pm}$ and Q_* in normal mode coördinates, so that Q_* cancels the identical term in $Q^{\pm}$ leaving $Q^{\pm\prime}$

$$R_E = K\frac{Q^{\pm\prime}}{Q_{Ax}Q_B}[Ax][B]\frac{kT}{h}e^{-E_0/RT} \qquad (3)$$

where K is the probability that the particle go on to products after it has once crossed the line above the saddlepoint. An alternate method, which is ultimately identical though quite different in the computational stages of the problem, is to express $Q^{\pm}/Q_{Ax}Q_B$ in terms of local valence-bond coördinates,[6] to express Q_* in terms of the reaction coördinate normal mode and to derive (appendix 1) the rate expression for a single reaction site and single electronic state

$$R_{HJR} = \frac{K''Z^{\pm\prime\prime}}{Z_{Ax}Z_B}[Ax][B]\nu^* e^{-E_0/RT} \qquad (4)$$

The configuration integrals are given in the recently-derived,[6] general, simple form

$$Z_{Ax} = \frac{(2\pi kT)^{(3N_1-6)/2}}{|F_s|_{Ax}^{1/2}}\prod_1^{N_1} J_a \qquad (5A)$$

$$"Z^{\pm}" = \frac{(2\pi kT)^{(3N-6)/2}}{|F_s|^{1/2}_{\pm}}\prod_1^{N} J_a \qquad (5B)$$

where N_1 is the number of atoms in the reactant Ax, N is the number of atoms in the activated complex, $|F_s|_{Ax}$ is the determinant of the force constant matrix for Ax in local valence bond coördinates, $|F_s|_{\pm}$ is the force constant matrix based directly on the various curvatures (as demonstrated in

(5) K. S. Pitzer and E. M. Mortensen, private communication.

(6) D. R. Herschbach, H. S. Johnston and D. Rapp, *J. Chem. Phys.* **31**, 1652 (1959).

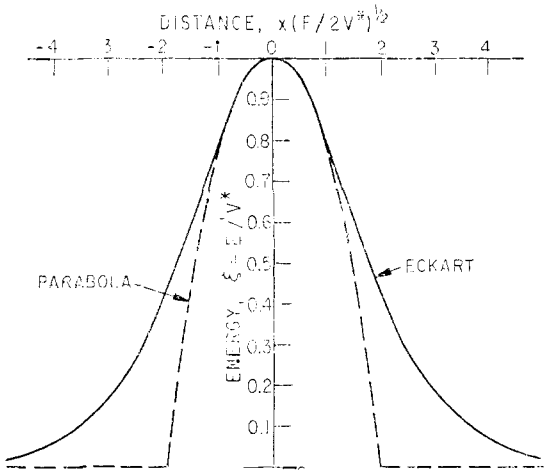

Fig. 3.—Symmetrical Eckart potential energy function and the truncated parabola with the same negative curvature at the maximum, F^*, and the same total height V^*. The plot of potential energy against distance is expressed in dimensionless form.

appendix 2) through the saddlepoint of the activated complex. (An expression similar to 5A applies to the other reactant.) In (4) ν^* is the imaginary "frequency of the reaction coördinate," and it is given by $(1/2\ \pi)(\lambda^*)^{1/2}$ where λ^* is the negative root of $|\mathbf{FG} - \mathbf{E}\lambda| = 0$ for the activated complex.[7] A general method for finding J_α and a convenient table for typical molecular groupings are given in ref. 6.

In case b, as defined above, that is, real vibrations of the reactants are quantized, we must include in the denominator a correction factor

$$\Gamma_i^{Ax} = (u_i/2)/\sinh(u_i/2) = Q_{qu}/Q_{cl} \qquad (6)$$

where $u_i = h\nu_i/kT$. For the vibrations of the activated complex orthogonal to the classical reaction normal mode, we may also add a factor $\Gamma_i^{\ddagger}$ of the same form as (6). However, here we encounter a conceptual difficulty; as pointed out by Kassel[8] the use of quantum mechanical stationary state partition functions for a species as transient as an activated complex is highly questionable. For the moment, bypassing this difficulty, the rate expression for classical reaction coördinate and quantized orthog onal vibrations is

$$\text{Rate} = \text{Rate (eq. 4)}\ \frac{\prod_{}^{3N-7}\Gamma^{\ddagger}}{\prod^{3N_{Ax}-6}\Gamma_{Ax}\ \prod^{3N_B-6}\Gamma_B} \qquad (7)$$

where the Γ's all have the form of eq. 6 .

One Dimensional Barrier Penetration.—In this section we wish to extend the work of Kemble,[9] Bell,[10] Eckart,[11] Shavitt[12] and others[3] by presenting the numerical and graphical results of the transmission coefficient as a function of energy and the distribution of transmitted systems from an incident packet of particles with a Boltzmann distribution of energies for the two potential energy barriers shown in Fig. 3. The solid line is a symmetrical Eckart[3] potential of height V^* and curvature $-F^*$ at the maximum

$$V(x) = \frac{V^*}{\cosh^2[x(F^*/2V^*)^{1/2}]} \qquad (8)$$

The dotted line in Fig. 3 is a truncated parabola with the same barrier height, V^*, and curvature, $-F^*$, as the Eckart potential.

$$V(x) = {}^*V - {}^1/_2F^*x^2 \qquad (9)$$

The Schroedinger equation for the Eckart potential can be solved, and for an incident particle of mass μ and energy E the transmission coefficient is

$$K(\xi) = \frac{\cosh(2\alpha\xi^{1/2}) - 1}{\cosh(2\alpha\xi^{1/2}) + \cosh(4\alpha^2 - \pi^2)^{1/2}} \qquad (10)$$

where $\xi = E/V^*$, $\alpha = 2\pi V^*/h\nu^*$ and $\nu^* = (1/2\pi)(F^*/\mu)^{1/2}$. If $4\alpha^2 >> \pi^2$ and for $\xi = 1$, the transmission function for the Eckart potential approaches the WKB solution for the parabolic barrier, which is[10]

$$K(\xi) = [1 + \exp\alpha(1 - \xi)]^{-1} \qquad (11)$$

As α approaches infinity one obtains high flat-topped barriers and consequently the transmission functions for both parabolic and Eckart barriers approach the classical form

$$K(\xi) = 0,\ \xi < 1;\ K(\xi) = 1,\ \xi > 1 \qquad (12)$$

The form of the transmission functions for the parabolic barrier for various values of α relative to a classical barrier is given in Fig. 4; similar curves for Eckart barriers are given in Fig. 5. Numerical

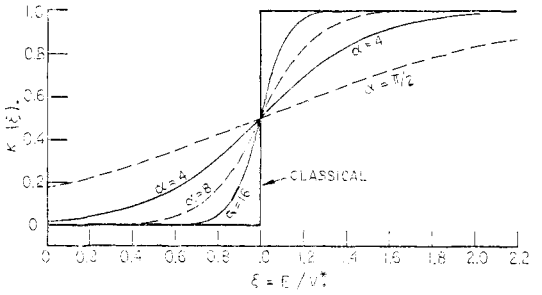

Fig. 4.—Transmission coefficients of a parabolic barrier as a function of the energy of an incident particle for various values of the parameter $\alpha = 2\pi V^*/h\nu^*$. For quantum mechanical systems, one notes reflections above the barrier as well as penetration beneath the barrier.

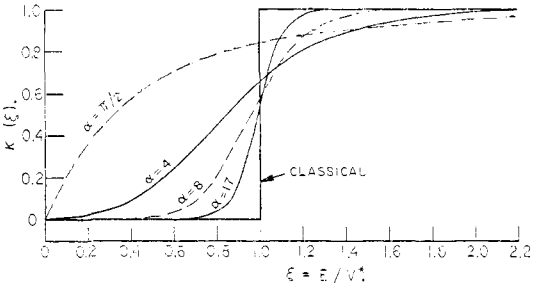

Fig. 5.—Transmission coefficients of an Eckart barrier as a function of the energy of an incident particle for various values of the parameter $\alpha = 2\pi V^*/h\nu^*$.

(7) E. B. Wilson, Jr., J. C. Decius and P. Cross, "Molecular Vibrations," McGraw-Hill Book Co., New York, N. Y., 1955.
(8) L. S. Kassel, *J. Chem. Phys.*, **3**, 399 (1935).
(9) E. C. Kemble, "Fundamental Principles of Quantum Mechanics," McGraw-Hill Book Co., New York, N. Y., 1937.
(10) R. P. Bell, *Trans. Faraday Soc.*, **55**, 1 (1959).
(11) C. Eckart, *Phys. Rev.*, **35**, 1303 (1930).
(12) I. Shavitt, *J. Chem. Phys.*, **31**, 1359 (1959).

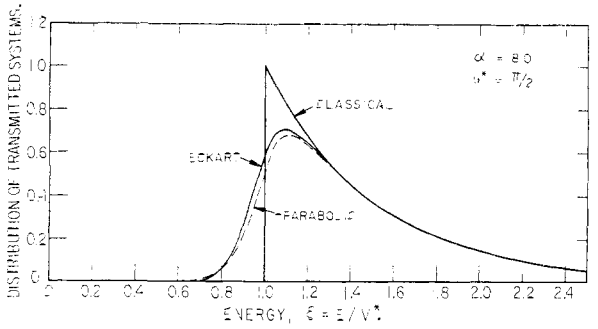

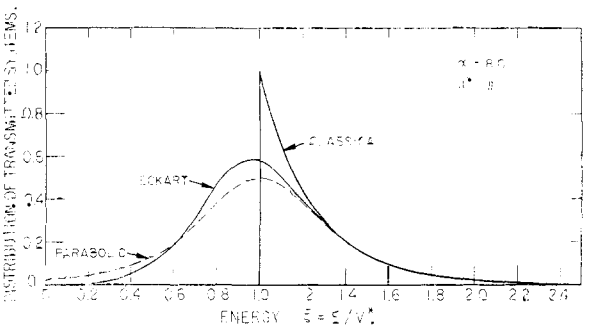

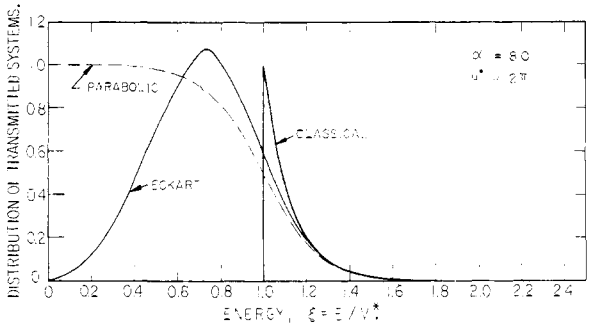

Figs. 6–8.—Distribution of systems transmitted through and over a barrier for an initial Boltzmann distribution of energies. For quantum mechanical systems the distribution of systems which pass is given for both parabolic and Eckart barriers, and the classical distribution is the same for each barrier, $\alpha = 2\pi V^*/h\nu^*$ and $u^* = h\nu^*/kT$ where $\nu^* = (1/2\pi)(F^*/m)^{1/2}$ and F^* is the absolute value of the negative force constant at the maximum. Relative areas under these and other similar curves give the data in Table II.

values for the transmission coefficient of the Eckart barrier as a function of α and u^* are given in Table I. It is noted that the transmission function $K(\xi)$ for the parabolic barrier is symmetrical with respect to inversion through $K = 1/2$, $\xi = 1$; and for low values of α, for example $\pi/2$, large degrees of tunnelling would occur below zero energies if the parabola were not truncated. The transmission function for the Eckart barrier goes to zero at zero energy. Another interesting feature of Figs. 4 and 5 is that quantum systems are reflected above the barrier as well as transmitted through the barrier. The net effect of this non-classical reflection and non-classical penetration is, as usual, given the name "tunnelling."

If a packet of particles, each of mass μ, and with an equilibrium distribution of energies proportional to $\exp(V^* - E)/kT = \exp[V^*(1 - \xi)/kT]$ is incident on the barrier of Fig. 3, the distribution function for transmitted systems is $K(\xi) \exp[V^*(1 - \xi)/kT]$, where $K(\xi)$ may be taken from (10) or (11). Under special conditions ($u^* < 2\pi$, $\alpha < V^*/kT$) the transmission function for the parabolic barrier may be integrated over a Boltzmann distribution of incident particles to give a closed expression. The corresponding integral for the Eckart potential does not seem to have a ready analytical solution; however, following the usual procedure,[12] we have evaluated it graphically and numerically with an IBM 704 computer for a number of cases of interest. Sample graphs of this sort for $\alpha = 8$ and for $u^* = \pi/2$, π and 2π for all three transmission functions are given in Figs. 6–8. These three figures correspond to a barrier height of about 6 kcal., an imaginary frequency of about 1600 i, and temperatures respectively 1500, 750 and 375° K. The ratio of the area under the Eckart distribution function in Figs. 6–8 to the area under the classical distribution curve gives the ratio of the number of transmitted systems in the Eckart case to the numbers expected from classical mechanics. This ratio is written as $\Gamma^* = k_{qu}/k_{cl}$. Values of Γ^* are given in Table II as a function of u^* and α. From Fig. 7 one sees that for $u^* = \pi$, the distribution of transmitted systems for the parabolic barrier is symmetrical about $\xi = 1$, that is, half the systems pass over the barrier and half tunnel through the barrier; this is true for all values of α, and the spread of energy of the transmitted systems goes up as α decreases.

In Fig. 6 the distribution curve for the parabolic barrier goes to zero at about $\xi = 0.5$; in Fig. 7 this curve has a small positive intercept at zero energy; in Fig. 8 very heavy tunnelling occurs at zero energy and would occur to energies of minus infinity except for truncation of the parabolic function. One is sure that the truncation shown in Fig. 3 is not a realistic picture of actual potential energy surfaces; the smooth continuous Eckart potential is much more nearly realistic. Thus we propose that the parabolic potential should not be used unless the distribution function, $K(\xi) \exp(V^* - E)/kT$, is essentially zero at $\xi = 0$. In this way the artificial truncation process need never be invoked. For larger degrees of tunnelling the Eckart potential is undoubtedly a better approximation. If the distribution function is essentially zero at $\xi = 0$, a condition safely observed if $u^* < \pi$ and $\alpha > 2$, then the parabolic barrier has the simple tunnelling correction function[10]

$$\Gamma^* = (u^*/2)/\sin(u^*/2); \quad u^* < \pi; \quad \alpha > 2 \qquad (13)$$

Finally, it is necessary in many cases to consider how the tunnelling factor Γ^* changes with temperature. The parameter θ^* is defined as

$$\theta^* = T \, \mathrm{d} \ln \Gamma^*/\mathrm{d}T \qquad (14)$$

For the parabolic barrier correction as given by (13) this function is $[(u^*/2) \cot (u^*/2) - 1]$.

Separable Reaction Coördinate.—Insofar as the primary making and breaking of a bond is concerned, an atom transfer reaction usually is discussed in terms of a potential energy contour plot

TABLE I

TRANSMISSION COEFFICIENT $K(\xi,\alpha)$ FOR SYMMETRICAL ECKART BARRIERS AS A FUNCTION OF INCIDENT ENERGY, $\xi = E/V^*$, AND FOR DIFFERENT VALUES OF $\alpha = 2\pi V^*/h|\nu^*|$

$\alpha\rightarrow$ / ξ	20	16	12	8	4	3	2	1	0.50	0.25	0.125
0.1	0.0_70	0.0_72	0.0_79	0.0_424	0.0_267	0.028	0.115	0.455	0.791	0.940	0.984
.2	$.0_70$	$.0_660$	$.0_521$	$.0_320$	.021	.070	.229	.633	.884	.969	.992
.3	$.0_71$	$.0_591$	$.0_424$	$.0_398$	.047	.129	.335	.728	.920	.979	.995
.4	$.0_646$	$.0_499$	$.0_318$	$.0_238$	.090	.201	.432	.787	.939	.984	.996
.5	$.0_692$	$.0_386$	$.0_211$	.012	.153	.287	.517	.826	.951	.987	.997
.6	$.0_314$	$.0_262$	$.0_255$	.036	.238	.379	.591	.855	.959	.990	.997
.7	$.0_216$	.038	.024	.090	.339	.471	.654	.877	.965	.991	.998
.8	.016	.184	.089	.201	.449	.558	.708	.893	.970	.992	.998
.9	.127	.539	.264	.375	.557	.637	.752	.906	.973	.993	.998
1.0	.531	.848	.551	.577	.655	.705	.790	.918	.976	.994	.998
1.1	.889	.961	.799	.749	.737	.762	.821	.927	.978	.994	.999
1.2	.981	.990	.924	.863	.803	.809	.848	.934	.980	.995	.999
1.3	.997	.998	.973	.928	.853	.847	.870	.941	.982	.995	.999
1.4	.999	.999	.990	.962	.892	.878	.889	.946	.983	.996	.999
1.5	1.000	1.000	.996	.980	.920	.902	.904	.951	.984	.996	.999
1.6	1.000	1.000	.998	.990	.941	.922	.918	.956	.986	.996	.999
1.7	1.000	1.000	.999	.994	.956	.937	.929	.959	.987	.996	.999
1.8	1.000	1.000	1.000	.997	.967	.949	.938	.962	.987	.997	.999
1.9	1.000	1.000	1.000	.998	.975	.959	.946	.965	.988	.997	.999
2.0	1.000	1.000	1.000	.999	.981	.966	.953	.968	.989	.997	.999

TABLE II

TUNNELLING FACTORS, $\Gamma^* = k_{qu}/k_{cl}$, FOR SYMMETRICAL ECKART POTENTIALS AS A FUNCTION OF $u^* = h|\nu^*|/kT$ AND α

u^*	$\alpha\rightarrow$ 20	16	12	8	4	3	2	1	0.5	0.25	0.125
1.5	1.1	1.1	1.1	1.16	1.18	1.20	1.22	1.19	1.12	1.06	1.03
2.0	1.2	1.2	1.2	1.24	1.30	1.31	1.32	1.27	1.16	1.08	1.04
3.0	1.5	1.5	1.5	1.56	1.58	1.60	1.57	1.43	1.25	1.12	1.06
4.0	2.0	2.0	2.0	2.04	2.02	2.00	1.91	1.61	1.34	1.17	1.08
5.0	3.2	3.21	3.07	2.94	2.69	2.57	2.34	1.83	1.44	1.22	1.10
6.0	6.11	5.69	5.21	4.54	3.69	3.38	2.90	2.09	1.55	1.26	1.13
7.0	14.9	12.3	9.90	7.60	5.23	4.52	3.62	2.38	1.67	1.31	1.15
8.0	46	32	22	13.8	7.60	6.15	4.55	2.72	1.80	1.37	1.17
9.0	199	107	55	27	11.3	8.48	5.76	3.11	1.94	1.42	1.20
10.0	....	437	162	57	17.3	11.9	7.34	3.56	2.09	1.47	1.22
12.0	....	....	....	307	42	24	12.1	4.68	2.42	1.60	1.27
14.0	....	....	....	....	110	50	20	6.19	2.81	1.73	1.32
16.0	....	....	....	....	304	107	34	8.19	3.25	1.87	1.37

on a R_1–R_2 diagram such as Fig. 1. On this diagram there are three extremes along the "classical reaction path," infinitely separated reactants, infinitely separated products, and the activated complex near the saddlepoint of the potential energy surface. In a Taylor series expansion about each of these three points, the three constant terms define: an origin of energy, the activation energy at absolute zero and the heat of reaction at absolute zero, not including zero point energy. The first derivative of each is zero by virtue of its being an extremum; and for sufficiently small displacements about each point the potential energy surface is adequately described by quadratic terms, as in eq. 1. It is only within the quadratic region that the vibrations are separable normal modes. For somewhat larger displacements the normal mode coördinates are recognizable and convenient, and they are used with corrections for the perturbing effect of "anharmonicity" and for slight coupling with respect to energy transfer. For even larger displacements the normal coördinates lose their identity and usefulness; the system in general becomes one of non-separable, interacting coördinates. The reaction coördinate is "separable" over the region near the saddlepoint where the potential energy surface may be regarded as quadratic as in eq. 1.

The rate expression for the separable parabolic reaction coördinate involves a tunnelling factor for the one dimensional normal mode

$$\Gamma^* = \int_0^\infty K_{qu}(E)\,P(E)\,dE \Big/ \int_0^\infty K_{cl}(E)\,P(E)\,dE \quad (15)$$

where the integral in the numerator is the area under the dotted curve in Fig. 6 or 7 and the denominator is the area under the classical curves on the same figures. The rate expression for the separable reaction coördinate is thus

$$\text{Rate (separable)} = R(\text{eq. 7})\,\Gamma^*(\text{eq. 13}) \quad (16a)$$

This equation can be expressed in the form

$$\text{Rate (separable)} = R(\text{classical, eq. 4})\,\frac{\Gamma_{3N-6}^{\ddagger}}{\prod\Gamma_{\text{reactants}}} \quad (16b)$$

In this way we see one of the advantages of expressing the rate in terms of the classical configuration integral with quantum corrections; the tun-

nelling factor for the separable reaction coördinate appears naturally as one of the $3N - 6$ quantum factors for the activated complex. It is an amusing coincidence that the quantum correction factors have the same form, $(u/2)/\sinh(u/2)$, where u is real for real vibrations, and for the reaction coördinate it is imaginary, converting $\sinh(u/2)$ to $\sin(u/2)$.

Another comparison of eq. 3 and 4 will be pointed out. When use is made of eq. 3, one goes to great pains to evaluate moments of inertia for the molecule as a whole or for internal rotors, if they are present. However, these moments of inertia always identically cancel mass terms in the complicated expressions for the product of vibrational frequencies in the classical limit of the vibrational partition function. Thus eq. 4 is equivalent to eq. 3, but with eq. 4 one never needs to compute moments of inertia and other terms which cancel. A common approximation in using eq. 3 is to treat vibrational partition functions as unity. If some vibrational frequencies are indeed low, then in effect one puts the moment of inertia in the numerator but fails to put the compensating terms in the low frequency vibrational partition function in the denominator. This approximation leads to substantial errors, up to a factor of 10^6, in polyatomic activated complexes.

Non-separable Reaction Coördinate.—If the de Broglie wave length associated with the atom being transferred is large compared to the quadratic portion of the potential energy surface, then the reaction coördinate is not separable from the real vibrations. In this section we wish to explore a simple, though inexact, method for handling this situation. We express the rate as

$$\text{Rate} = \text{Rate (eq. 7)} \frac{\int \cdots \int_0^\infty K_{qu}(q,E)P(E)dq_1 \cdots dq_r dE}{\int \cdots \int_0^\infty K_{cl}(q,E)P(E)dq_1 \cdots dq_r dE} \quad (17)$$

where $K_{qu}(q,E)$ is the quantum mechanical transmission coefficient of a particle with energy E (relative to reactants) and coördinates q arriving from reactants, $K_{cl}(q,E)$ is the classical transmission coefficient (zero or one) and $P(E)$ is the probability of energy E in the coördinates q.

When A and B are heavy atoms or groups and x is H or D, we have the simplest case with which to test (17). Normal mode analysis (with $F_{Ax}^{\ddagger} = F_{xB}^{\ddagger}$) gives a reaction coördinate in which $dR_{Ax} = -dR_{xB}$, that is, R_{AB} remains constant and x moves from A to B with a small motion of A–B to conserve center of mass. The reduced mass of this motion is essentially $m_x/2$ (the factor of 2 arises because a single unit of motion of x adds to R_{Ax} and subtracts from R_{xB} to give a double motion in $dR_{Ax} - dR_{xB}$) This coördinate corresponds to motion through the saddlepoint with a slope of $-45°$. Any other angle of crossing corresponds to forced motions of the heavy end groups, A and B, and to a much higher effective mass. Thus the integration in (17) can be carried out for different values of the crossing point, but in all cases for a $-45°$ crossing angle, as between GH and LM of Fig. 1. The "approximate method" mentioned in the introduction is that the line through each such crossing point is treated as a quasi-one dimensional symmetrical Eckart-potential tunnelling problem.

Dr. Weston evaluated in detail a potential energy surface for the H–H–H reaction.[4] He has kindly let us borrow his detailed numerical values of the potential energy function. We are using these data to explore the effect of large scale tunnelling. The saddlepoint for H_3 is at 0.93–0.93Å. The reaction normal mode is a straight line of $-45°$ slope through 0.93–0.93, EOF of Fig. 1. The energy profile of such a straight line is given to scale in Fig. 2 as EOF. A parabola with the same curvature at 0.93–0.93 is included in Fig. 2, and we see that the quadratic region along this energy profile is about ± 0.3 Å.; the de Broglie wave length of a hydrogen atom at 500°K. is 0.78 Å. The extended reaction coördinate EOF encounters side-wall repulsion and eventually turns upward. The minimum energy is 1.4 kcal. below the saddlepoint, ΔV^* of Fig. 2, while the energy of reactants is 8.6 kcal. below the saddlepoint. Parallel cuts ($-45°$) at different crossing points, 0.96–0.96 (LM), 0.90–0.90 (GH) are shown in Figs. 1 and 2. For crossing points snorter than the saddlepoint, GH, the curvature is less sharp (smaller F^*), the energy from crossing point to minimum is less deep (smaller ΔV^*) and the crossing point is higher than at the saddlepoint; all of these effects tend to decrease the tunnelling for short crossings. For crossing points longer than the saddlepoint, LM, F^* is greater and ΔV^* is greater than at the saddlepoint; these effects tend to give more tunnelling than at the saddlepoint. However, the height of the barrier increases as one moves away from the saddlepoint, and this effect *via* Boltzmann's factor tends to counteract the more favorable trend in F^* and ΔV^*.

A series of cuts at $-45°$ was made for crossing points varying every 0.01 Å. from 0.80, 0.80; 0.81, 0.81 . . . 0.93, 0.93; . . . 1.09, 1.09. For each such cut a value of F and ΔV was found and at each of three temperatures, 333, 500 and 1000°K., μ^* and α were evaluated for H–H–H and D–D–D. For each such cut the Eckart transmission coefficient from Table II is interpreted as the value for $K(q)$, where q is the crossing point for a $-45°$ motion. The plot of $K(q)$ against q is given in Figs. 9, 10, 11 for H–H–H and D–D–D at each of three temperatures. The form of the classical curve is given by the Boltzmann factor for the crossing point, and all transmissions are normalized to unity for classical transmission just at the saddlepoint. The area under the classical curve is the denominator of eq. 17, and the area under the quantum curves is the numerator of eq. 17. Thus the relative areas give an estimate of a two-dimensional tunnelling correction, $\Gamma^*_{non-sep}$.

Using Figs. 9–11 we can evaluate tunnelling correction factors by the several different methods and compare the results in Table III. The ratios of quantum to classical areas under the curves in Figs. 9–11 are entered as Γ^*_{av}. If we take these to be the best estimate of tunnelling, we see that at low temperatures a parabolic correction greatly overestimates tunnelling, and a one dimensional Eckart correction based on the reaction path (AOB, in Fig. 1) also greatly overestimates tunnelling.

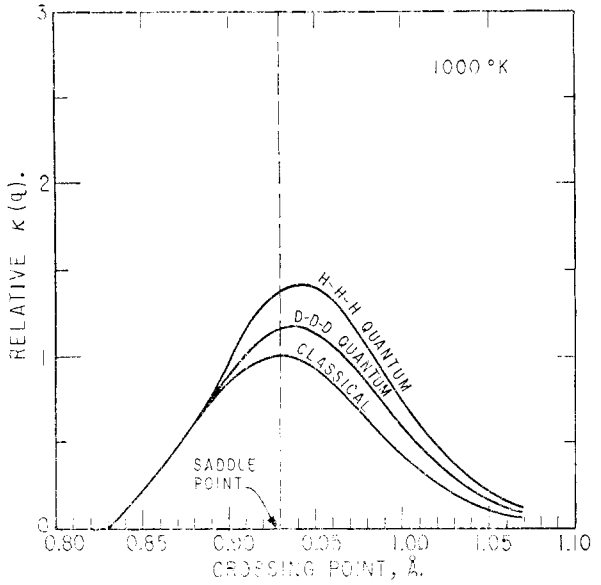

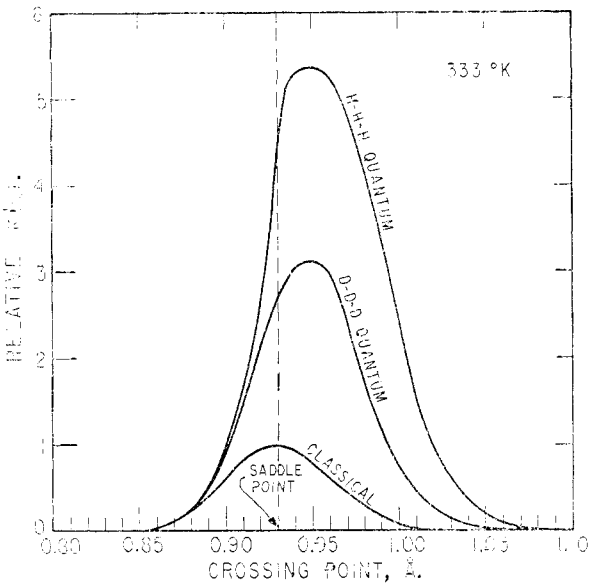

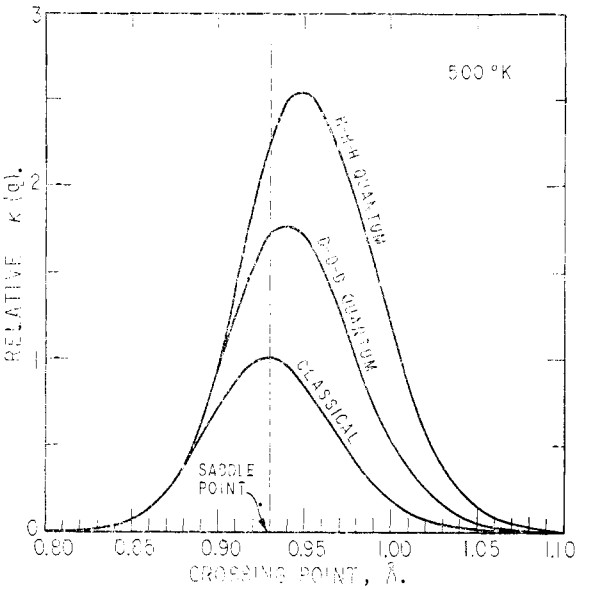

Figs. 9–11.—Relative rates of barrier crossing for various lines between HG and LM in Fig. 1. Each value of $K(q)$ corresponds to the area under a curve such as Figs. 6–8. Calculations are made for the H_3 reaction and the D_3 reaction. Relative areas under these curves give the values of $\Gamma^*_{av.}$ in Table III. Relative values at the saddlepoint give $\Gamma^*_{r.c.}$ Relative values at the maxima give $\Gamma^*_{m.p.}$

A one dimensional Eckart correction based on the normal mode coördinate (EOF in Fig. 1) fairly seriously underestimates the tunnelling correction. One fortunate simplification emerges; the values of K(q) for the *most probable* crossing point on CD in Fig. 1 that give the maximum in Figs. 9–11 are in rather good agreement with the tunnelling factor based on the averages. (This feature is not uncommon: the average is well approximated by the most probable situation.) The carrying out of the computations to construct Figs. 9–11 is very tedious. The constructive simplification discovered by this analysis and used to interpret experimental data is to replace the averages in (17) by most probable values, to give the practical, working relation

Rate (non-sep) = R(eq. 7)Γ^* (2 dim., most prob.) (18)

Other aspects of Figs. 9–11 are worthy of comment. At 1000°K., both classically and in terms of quantum mechanics, the systems which react were widely distributed in crossing points and the classical and quantum distributions differ only slightly. At low temperatures the Boltzmann factor sharpens the classical distribution of systems which react and tunnelling becomes of much greater

TABLE III

COMPARISON OF TWO-DIMENSIONAL TUNNELLING FACTORS WITH VARIOUS ONE-DIMENSIONAL TUNNELLING FACTORS

Reaction	Corrections	Tunnelling factors $\Gamma^* = k_{qu}^*/k_{cl}^*$ 333°K.	500°K.	1000°K.
H-H-H	[a]	5.84	2.66	1.41
	[b]	5.31	2.54	1.41
	[c]	3.85	2.20	1.38
	[d]	16.5	3.75	1.40
	[e]	...	6.4	1.40
D-D-D	[a]	3.20	1.80	1.19
	[b]	3.13	1.76	1.18
	[c]	2.70	1.70	1.17
	[d]	4.6	1.9	1.18
	[e]	12.8	2.02	1.18
H-H-H	[a]	1.82	1.48	1.19
D-D-D	[b]	1.70	1.44	1.20
	[c]	1.43	1.30	1.18
	[d]	3.60	1.97	1.18
	[e]	...	3.16	1.18

[a] $\langle\Gamma^*\rangle_{av}$, tunnelling factor averaged over various crossing points, two dimensional average, the area under quantum curve divided by area under classical curve in Figs. 9, 10, 11. [b] $\Gamma^*_{m.p.}$, the value of $\Gamma^*(q)$ at the *most probable* crossing point, the maximum value of K(q) in Figs. 9, 10, 11. [c] $\Gamma^*_{r.c.}$, the value of K(q) along the *reaction coördinate* normal mode through the saddlepoint; the value of K(q) at 0.93 in Figs. 9, 10, 11; note that ΔV^* in the Eckart relation is 1.3 kcal., giving a low value of α. [d] $\Gamma^*_{r.p.}$, the value of K(q) along the "classical reaction path" extending from reactants to complex to products. The value of ΔV^* is the full ΔV^*_{act} or 7.8 kcal. The Eckart parameter α is thus much larger than for (c), although the F^*, μ, ν^*, or u^* are all the same. The difference between (c) and (d) is due to the importance of "side wall repulsions" to extended normal mode tunnelling. [e] Bell's parabolic relation, eq. 13.

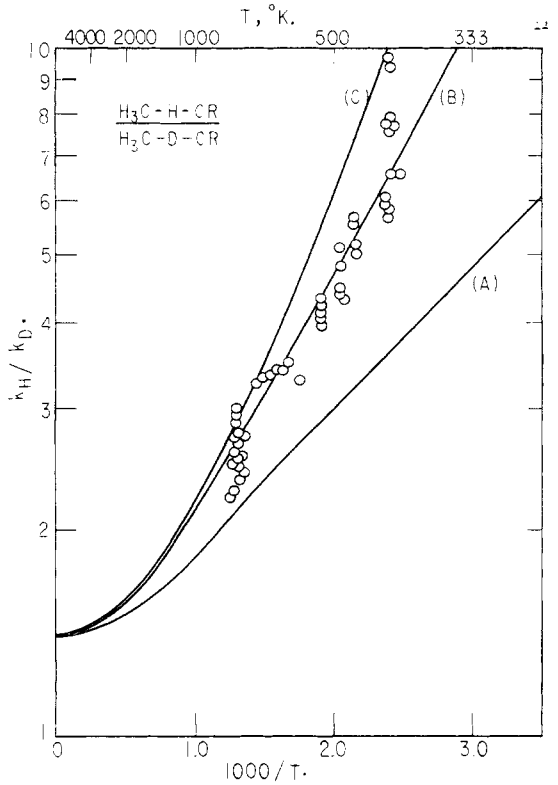

Fig. 12.—Calculated and observed kinetic isotope effect for methyl radical reactions with organic compounds. (A) Calculated curve assuming no tunnel effect, where the kinetic isotope effect arises largely from $(m_D/m_H)^{1/2}$ and zero point energy differences of reactants. (B) Calculated curve assuming tunnel effect based on $\Gamma^*_{m.p.}$ as found from treatments similar to but less extensive than Figs. 9–11. (C) Calculated curve assuming Eckart potential along AOB of Fig. 1 and α given by $2\pi V^*_{act}/h\nu^*$.

relative importance. However, at low temperatures the Boltzmann factor largely wins out over the tunnelling phenomenon with respect to locating the reaction sites. The most probable classical crossing point is 0.93–0.93, and at 333°K. the most probable quantum reaction trajectory is through 0.95–0.95. Even at the lowest temperatures, where the tunnelling factor is almost 6, the distribution function for quantum systems which cross the symmetric stretch axis is surprisingly similar to that for classical systems. The nature of the London–Eyring–Sato potential energy surface is such that the reaction process is much more nearly along the classical normal mode than one would expect, simply from a comparison of the de Broglie wave length and the region of separability.

Methyl Radical–Hydrocarbon Kinetic Isotope Effects.—For the family of reactions

$$x_3C + y\text{-}CR$$

where x is H or D and y is H or D, a portion of the Sato potential energy surface was evaluated. The activation energy (corrected for zero point energy) was taken to be 13.6 kcal.[2] The activated complex was assumed to have $R_1 = R_2$, and the saddlepoint was estimated from Pauling's rule of bond order-bond distance to be near $\rho = \Delta R = 0.18$ Å. For various values of Sato's parameter k between 0.10 and 0.20 and for values of ρ between 0.15 and 0.25, a relatively small number of potential energy points were evaluated, and the correct saddlepoint was quickly found to be given by

$$k_{Sato} = 0.110;\ \rho = 0.22\ \text{Å}. \qquad (19)$$

A more extensive calculation of the line EOF (Fig. 1) gives a curve analogous to EOF in Fig. 2 where $\Delta V^* = 3.0$ kcal. and $F^* = 1.04 \times 10^5$ dynes/cm. A similar calculation through a pair of lines, such as LM, parallel to EOF and close to it, established the most probable reaction path to be only about 0.014 Å. removed from the normal mode path at 500°K., the center of the data. The same line was used to calculate tunnelling at all temperatures, even though it is realized that this may slightly underestimate the tunnelling at low temperatures. The data from the literature for the reactions[13] of methyl radicals with acetone and ethane to abstract H or D were reviewed extensively in T-I. The vibration frequencies of the activated complex were computed in T-I, and these will be used again. Also in T-I we calculated the tunnelling correction using an Eckart potential along line AOB.

In Fig. 12 we see the experimental points, the curve (A) which includes no tunnelling correction (curve A is dominated by the differences of R–H and R–D in the *reactants*, and it is very little affected by any assumptions about the activated complex), curve (C) which includes a tunnelling correction based on AOB, as if the mass were constant along this line ($\Gamma^*_{r.p.}$), and curve (B) which is based on eq. 18. The experimental scatter is discouragingly large. However, we feel this analysis may indicate the important factors in large tunnelling corrections in reactions of the type: heavy group–hydrogen–heavy group. The heavy end groups constrain the tunnelling motion to be along a straight line of −45° slope in Fig. 1. A consideration of tunnelling over all the area GLMH in Fig. 1 shows that most of it occurs over a band such as ELMF, which is about 0.1 Å. wide. Tunnelling cannot occur from A to B because of the very high barrier opposing a −45° motion between these points. Tunnelling cannot occur around the curve from A to B because any motion other than the −45° line forces the heavy end groups to move, and their mass is so great that their tunnelling is negligible. By the time the system has moved up to where it can get a good tunnelling path near EOF, it has almost gone to the top of the barrier anyhow. Thus we picture the reaction process as activation by collision up to region E or L in Fig. 2, and then a quantum mechanical barrier penetration, reflection or overflight across the area ELMF. Curve (B) in Fig. 12 is based on this model, and it provides a reasonable representation of the data.

Acknowledgments.—We are very grateful to Dr. Ralph Weston for providing us with a complete Sato potential energy surface for H_3. Also we are

(13) E. W. R. Steacie, "Atomic and Free Radical Reactions," Sec. Ed., Reinhold Publishing Corp., New York, N. Y., 1954; J. R. McNesby and A. S. Gordon, THIS JOURNAL, **76**, 823, 1416 (1954); F. O. Rice and T. A. Vanderslice, *ibid.*, **80**, 291 (1958).

indebted to the Alfred P. Sloan Foundation for a Fellowship in support of this study.

Appendix I

Derivation of Equation 4.—The derivation of eq. 4 follows very closely the derivation of eq. 15a of ref. 6, HJR, except that it is for an activated complex, for which one separable normal mode is the unstable motion above an inverted parabola between limits $-\delta/2$ to $\delta/2$. The classical partition function for this normal mode is

$$Q^* = \frac{1}{h}\int_{-\delta/2}^{\delta/2} e^{-f^*q^2/kT}\,\mathrm{d}q \int_{-\infty}^{\infty} e^{-p^2/2m^*kT}\,\mathrm{d}p \quad (21)$$

where q is the reaction normal mode coördinate, p is the reaction normal mode momentum, f^* is the force constant of the reaction normal mode and is a negative number and m^* is the mass associated with the reaction normal mode. Defining the first integral in (21) as Δ and evaluating the second integral, we get

$$Q^* = (1/h)\,\Delta\,(2\pi m^* kT)^{1/2} \quad (22)$$

The classical partition function for the entire activated complex (regarded as non-linear and with N atoms) is (*cf.* HJR, eq. 3)

$$Q_{\mathrm{class}} = Z \prod_{\alpha=2}^{N} h^3/(2\pi m_\alpha kT)^{1/2} \quad (23)$$

where m_α refers to atomic masses. The complete partition function in terms of 3 N normal modes (including rotations and translations as normal modes) is (*cf.* HJR, eq. 10)

$$Q_{\mathrm{class}} = V8\pi^2(2\pi kT/h^2)^3 M^{3/2}|I|^{1/2} \prod_{i=1}^{3N-7} u_i^{-1}\, Q^*$$

where Q^* is given by 22. A comparison of eq. 23 and 24 shows that the configurational integral is (*cf.* HJR, eq. 11)

$$Z = \frac{V8\pi^2 M^{3/2}|I|^{1/2} \prod_{i=1}^{3N-7} u_i^{-1}}{\Pi m_\alpha^{3/2}(2\pi kT)^{3N-6/2}}\, u^*Q^* \quad (24)$$

where the product of u is raised from $3N-7$ to $3N-6$ by multiplying and dividing by $u^* = h\nu^*/kT = h(f/m^*)^{1/2}/2\pi kT$. In a vibrational analysis we again obtain $[F_s]\,[G_s] = \prod_{i=1}^{3N-6} \lambda_i$, where F_s and G_s refer to local valence bond properties, and $\lambda_i = (2\pi\nu_i)^2$. The product of the last two terms in (24) gives considerable cancellation

$$u^*Q^* = f^*\Delta/(2\pi kT)^{1/2} \quad (25)$$

From (21) we see that Δ is a function only of f^* and T; it is not a function of mass. Consequently we again have a separation of mass and force-constant variable in analogy to (HJR eq. 13a, b).

$$J_s = \frac{V8\pi^2 M^{3/2}|I|^{1/2}}{\Pi m_\alpha^{3/2}|G_s|^{1/2}} = \frac{Z|F_s|^{1/2}}{(2\pi kT)^{3N-6/2}}\,\frac{(2\pi kT)^{1/2}}{f^{*1/2}\Delta} \quad (26)$$

The first identity in J does not depend on force constants, the second does not depend on mass, and therefore both the first and second identities depend on neither. Thus the first identity depends on the geometry of the activated complex as if it were a normal molecule, and the table of J's in HJR is directly applicable to the activated complex structure. The configurational integral for the activated complex is

$$Z^{\ddagger} = \left[\frac{(2\pi kT)^{3N-6/2}}{|F_s|^{1/2}} \prod_{\alpha=1}^{N} J_\alpha\right] \frac{f^{*1/2}}{(2\pi kT)^{1/2}} \quad (27)$$

or, defining "$Z^{\ddagger}$" as in eq. 5B we have

$$Z^{\ddagger} = \text{"}Z^{\ddagger}\text{"}\, f^{*1/2}\,\Delta/(2\pi kT)^{1/2}$$

Replacing $Q^{\ddagger}/Q_{\mathrm{Ax}}Q_{\mathrm{B}}$ in (2) by $Z^{\ddagger}/Z_{\mathrm{Ax}}Z_{\mathrm{B}}$ we get cancellation of Δ, kT, and h

$$R = [\mathrm{Ax}][\mathrm{B}]\,\frac{\text{"}Z^{\ddagger}\text{"}}{Z_{\mathrm{Ax}}Z_{\mathrm{B}}}\,\frac{f^{*1/2}}{2\pi m^{*1/2}}\,e^{-E_0/RT} \quad (28)$$

But the symbols $(f^*/m^*)^{1/2}/2\Pi$ are just the definition of ν^*, the imaginary frequency in the reaction coördinate. Upon substitution for ν^*, we get eq. 4.

Appendix 2

Evaluation of Force Constant Determinant of Activated Complex from a Potential Energy Surface.—From the derivation above, we see that the force constant determinant required in eq. 5B can be obtained directly from a potential energy surface. For a linear three-atom complex and with a R_1–R_2 plane such as Fig. 1, the stretching force constants about the atom transferred are given directly by various curvatures through the saddlepoint. The coefficient F_{11} of eq. 1 is given by $2\Delta V = F_{11}\Delta R_1^2$ for a line through O, parallel to the R_1 axis, so that $\Delta R_2 = 0$. The coefficient F_{22} is given by $2\Delta V = F_{22}\Delta R_2^2$ along a line through O parallel to the R_2 axis. To obtain F_{12}, we must find the curvature through some line not parallel to R_1 or R_2; either COD or EOF is very convenient for this purpose, although other lines through O of slope c may be used. If $c = \mathrm{d}R_2/\mathrm{d}R_1$, the general expression for changes in potential energy from the saddlepoint becomes, along this line

$$2\,\mathrm{d}V = (F_{11} + c^2F_{22} + 2cF_{12})(\mathrm{d}R_1)^2 \quad (29)$$

The square of the distance along this line is

$$(\mathrm{d}y)^2 = (\mathrm{d}R_1)^2 + (\mathrm{d}R_2)^2 = (1 + c^2)(\mathrm{d}R_1)^2 \quad (30)$$

The force constant along this line is

$$F_c = 2\,\mathrm{d}E/(\mathrm{d}y)^2 = (F_{11} + c^2F_{22} + 2cF_{12})/(1 + c^2)$$

The value of the interaction constant is

$$F_{12} = \frac{F_c(1 + c^2) - F_{11} - c^2F_{22}}{2c} \quad (31)$$

For the special case that $F_{11} = F_{22}$

$$F_{12} = \frac{(1 + c^2)(F_c - F_{11})}{2c} \quad (32)$$

For the special case of (31) that $c = -1$, for example, EOF in Fig. 1

$$F_{12} = (F_{11} + F_{22})/2 - F_{-1} \quad (33)$$

For the special case of (32) that $c = -1$ and $F_{11} = F_{22}$

$$F_{12} = F_{11} - F_{-1} \quad (34)$$

The force constant determinant in eq. 4 is thus evaluated

$$|F_s| = \begin{vmatrix} F_{11} & F_{12} \\ F_{12} & F_{22} \end{vmatrix} = F_{11}F_{22} - F_{12}^2 \quad (35)$$

For a saddlepoint with one negative curvature, the expression $F_{11}F_{22} - F_{12}^2$ is negative, and thus its square root in eq. 4 is imaginary, cancelling the imaginary factor in ν^*. The factor w^2 which "diagonalizes" F_s is $(1 - F_{12}^2/F_{11}F_{22})$, (*cf.* HJR eq. 16).

The G-determinant can be taken from the geometry of the activated complex in the usual way, ref. 7. The secular equation $[\mathbf{FG} - \mathbf{E}\lambda] = 0$ can be solved for the negative value of λ^*, without necessity of finding the other roots. From this value of λ^*, we find ν^*, to substitute into eq. 4. The other roots of the secular equation give the frequencies required for eq. 7, if quantum corrections are needed for the real vibrations.

From this analysis we illustrate that in order to calculate a rate according to activated complex theory, we do not need the entire potential energy surface but only a small segment of it near the saddlepoint. If the de Broglie wave length is small compared to the region of separability, that is, the quadratic region, we use eq. 7 to calculate the rate, and all we need is the location of the saddlepoint and its infinitesimal curvatures there. For large degrees of tunnelling, larger portions of the potential energy surface are needed, as discussed in the body of this paper.